Ion-atom-atom three-body recombination in cold hydrogen and deuterium plasmas

Miruna T. Cretu,[1] Marjan Mirahmadi [ORCID],[1] and Jesús Pérez-Ríos [ORCID][1,2,3]

[1]*Fritz-Haber-Institut der Max-Planck-Gesellschaft, Faradayweg 4-6, D-14195 Berlin, Germany*
[2]*Department of Physics, Stony Brook University, Stony Brook, New York 11794, USA*
[3]*Institute for Advanced Computational Science, Stony Brook University, Stony Brook, New York 11794-3800, USA*

We present a detailed study about ion-atom-atom three-body recombination in hydrogen and deuterium plasmas based on classical trajectory calculations in hyperspherical coordinates. Our results, due to the predominant role of the long-range charged-induced dipole interaction, indicate that H_2^+ and D_2^+ are the main reaction products in the case of hydrogen and deuterium plasmas, respectively. In addition, we find a more steep energy-dependent reaction rate when the collision energy surpasses the dissociation energy of the molecular ion, thus entering a new dynamical regime dominated by short-range interactions.

I. INTRODUCTION

Three-body recombination is the chemical process in which three atoms collide to form a molecule as a product state. These reactions are relevant in many different areas of physics and chemistry. For instance, in ultracold gases they play a decisive role on the stability of a quantum gas [1–7]; in hybrid atom-ion traps, they lead to new charged products [8–11]; in chemical physics, they are necessary to understand the formation of van der Waals molecules [12–20]; in astrophysics, they are responsible for the formation of H_2, one of the most important coolants regarding star formation [21,22]. In the same vein, in plasmas, where ions, electrons, and neutral atoms live together, three-body recombination of electrons and protons, $e + e + H^+ \rightarrow H + e$, plays a vital role as one of the main mechanisms of plasma recombination [23–25].

Among different three-body processes, ion-atom-atom three-body recombination is especially interesting since it involves two possible product states: (i) molecular ion formation, $A + A + A^+ \rightarrow A_2^+ + A$ and (ii) molecular formation, $A + A + A^+ \rightarrow A_2 + A^+$ [26]. Recently, this reaction has been studied by applying a classical trajectory method in hyperspherical coordinates [7,27,28], finding a threshold law [10] showing the dominance of molecular ion formation concerning neutral molecules [8,29] at low collision energies. These have been experimentally confirmed in hybrid atom-ion traps experiments [11,30]. However, in the plasma physics front, despite the presence of ions and neutrals, the study of ion-atom-atom three-body recombination has received little theoretical and experimental attention, barring the work of Krstić *et al.* [31].

This paper presents a first-principles calculation of the ion-atom-atom three-body recombination rate in hydrogen and deuterium plasmas in a wide range of temperatures relevant to cold plasma physics. As a result, this work can be viewed as extending our previous work on ion-atom-atom three-body recombination, going into the high-energy regime, where short-range physics starts to play a role. A classical trajectory method in hyperspherical coordinates is employed, based on ideas pioneered by Smith [32]. Monte Carlo sampling of trajectories is used to calculate the opacity function—the reaction probability as a function of the collision energy and impact parameter—and the three-body recombination cross section, which is conducive to calculating the recombination rate. The study led to the expected preponderance of molecular ion formation to the detriment of neutral molecules, although molecules are formed in the whole range of temperatures under consideration. These results are further discussed in the framework of tokamak physics, particularly its implications regarding the ultimate divertor detachment stage.

II. THEORETICAL TREATMENTS AND COMPUTATIONAL DETAILS

Consider a system of three particles (see Fig. 1) with masses m_i and positions $\vec{r}_i$ ($i = 1, 2, 3$) interacting via the potential $V(\vec{r}_1, \vec{r}_2, \vec{r}_3) = U(r_{12}) + U(r_{23}) + U(r_{31})$, where $r_{ij} = |\vec{r}_j - \vec{r}_i|$. The Hamiltonian governing the particles' motion reads as

$$H = \frac{\vec{p}_1^2}{2m_1} + \frac{\vec{p}_2^2}{2m_2} + \frac{\vec{p}_3^2}{2m_3} + V(\vec{r}_1, \vec{r}_2, \vec{r}_3), \quad (1)$$

where $\vec{p}_i$ are the momentum vectors of the *i*th particle. To more conveniently solve Hamilton's equations and study the classical scattering of the three particles, the problem is treated in Jacobi coordinates,

$$\vec{\rho}_1 = \vec{r}_2 - \vec{r}_1,$$
$$\vec{\rho}_2 = \vec{r}_3 - \frac{m_1 \vec{r}_1 + m_2 \vec{r}_2}{m_1 + m_2}, \quad (2)$$
$$\vec{\rho}_{CM} = \frac{m_1 \vec{r}_1 + m_2 \vec{r}_2 + m_3 \vec{r}_3}{M},$$

where $M = m_1 + m_2 + m_3$ is the total mass of the system and $\vec{\rho}_{CM}$ is the three-body center-of-mass vector. As the total linear momentum is conserved, the degrees of freedom of the center of mass are neglected and the Hamiltonian from Eq. (1) is expressed as

$$H = \frac{\vec{P}_1^2}{2\mu_{12}} + \frac{\vec{P}_2^2}{2\mu_{3,12}} + V(\vec{\rho}_1, \vec{\rho}_2). \qquad (3)$$

Here, $\mu_{12} = m_1 m_2/(m_1 + m_2)$, $\mu_{3,12} = m_3(m_1 + m_2)/M$ and $\vec{P}_1$, $\vec{P}_2$ indicate the conjugated momenta of $\vec{\rho}_1$ and $\vec{\rho}_2$, respectively. $V(\vec{\rho}_1, \vec{\rho}_2)$ is the interaction potential expressed in terms of Jacobi coordinates.

Solving Hamilton's equations of motion for the three-body problem as a function of Jacobi coordinates allows the characterization of the system in three-dimensional (3D) space. Alternatively, it is desirable to study the dynamics of the same system in a six-dimensional (6D) space, where it can be mapped into a single particle. This is made possible by the pioneering work of Smith [32], which allows the construction of 6D position and momenta vectors. Hyperspherical coordinates are employed for the representation of the 6D vectors and a definition of the impact parameter in 6D space follows. That is, the impact parameter $\vec{b}$ is defined as a component of the position vector lying in the hyperplane perpendicular to the initial momentum $\vec{P}_0$ and is obtained as a result of the Gram-Schmidt orthogonalization procedure.

Thus, an expression for the classical cross section, as a prerequisite for the recombination rate relation, is obtained after averaging out the hyperangular degrees of freedom [7,28],

$$\sigma_{\text{rec}}(E_c) = \int \mathcal{P}(E_c, \vec{b}) b^4 db d\Omega_b$$
$$= \frac{8\pi^2}{3} \int_0^{b_{\max}(E_c)} \mathcal{P}(E_c, b) b^4 db, \qquad (4)$$

where E_c is the collision energy and $d\Omega_b = \sin^3(\alpha_4^b)\sin^2(\alpha_3^b)\sin(\alpha_2^b)d\alpha_4^b d\alpha_3^b d\alpha_2^b d\alpha_1^b$ is the solid angle element associated with vector $\vec{b}$. The function $\mathcal{P}(E_c, b)$ is the so-called opacity function and it defines the probability that a particular trajectory at collision energy E_c and impact parameter b leads to a recombination event. $b_{\max}$ represents the largest impact parameter for which three-body recombination events occur, i.e., $\mathcal{P}(E_c, b) = 0$ for $b > b_{\max}$. Finally, the energy-dependent three-body recombination rate is introduced as

$$k_3(E_c) = \sqrt{\frac{2E_c}{\mu}} \sigma_{\text{rec}}(E_c). \qquad (5)$$

Therefore, after starting with a given set of initial conditions $\vec{\rho}_0$, R, $\vec{b}$, and $\vec{P}_0$, the method relies on mapping the conditions in 3D space to solve Hamilton's equations in Jacobi coordinates. Following that, the resulting momenta and positions are mapped back into the 6D space where the classical three-body cross section is defined by Eq. (4).

The integral in Eq. (4) is evaluated by employing the Monte Carlo integration method [27]: The initial hyperangles determining the orientation of vectors $\vec{P}_0$ and $\vec{b}$ in 6D space are randomly sampled from their appropriate angular
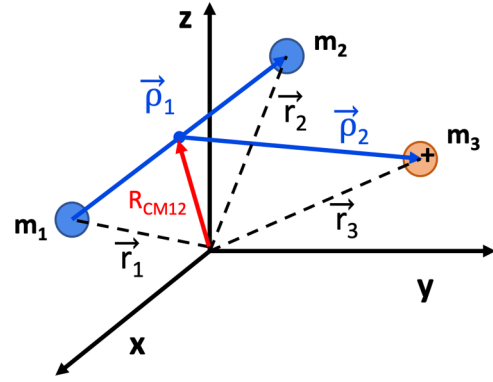

FIG. 1. Jacobi coordinates for the three-body problem, where the third particle is charged, and R_{CM12} indicates the center of mass of particles 1 and 2.

distribution functions in 6D and the opacity function $\mathcal{P}(E_c, \vec{b})$ is subsequently averaged over the hyperangles. This is achieved by running n_t trajectories and counting the number of trajectories n_r that lead to recombination events. Thus,

$$\mathcal{P}(E_c, b) \approx \frac{n_r(E_c, b)}{n_t(E_c, b)} \pm \frac{\sqrt{n_r(E_c, b)}}{n_t(E_c, b)} \sqrt{\frac{n_t(E_c, b) - n_r(E_c, b)}{n_t(E_c, b)}}, \qquad (6)$$

where the latter term in Eq. (6) is the statistical error associated with the Monte Carlo method.

Hamilton's equations are solved using the ode113 solver in MATLAB, with absolute and relative tolerances of 10^{-15} and 10^{-11}, respectively. The conservation of the total energy and of the magnitude of the total angular momentum vector during collisions is ensured to at least four and six significant digits, respectively. Last but not least, the initial magnitude of the hyperradius ($\vec{\rho}_0$) is generated randomly from the interval $[R_0 - 50, R_0 + 50] \, a_0$, where $R_0 = 40 \, a_0$ and a_0 is the Bohr radius. R_0 is chosen so the three particles are initially found in an uniform rectilinear state of motion.

The number of partial waves contributing to the scattering observables can be used as a measure of the validity for the classical trajectory method. By knowledge of the long range of the interaction potential (V_l) and by solving $E_c = V_l(R^*)$ for a given kinetic energy E_c. Therefore, R^* is the distance where V_l shows a maximum, and the largest l value can be approximated, which determines the number of partial waves contributing to the scattering. For atom-ion collisions, the long range of the interaction potential reads as (in atomic units):

$$V_l(R) = -\frac{\alpha}{2R^4} + \frac{l(l+1)}{2\mu R^2}, \qquad (7)$$

where l is the angular momentum quantum number associated to the relative motion, α is the polarizability of the atom, and μ is the reduced mass of the colliding pair. Figure 2 shows the magnitude of the maximum l value ($l_{\max}$) as a function of collision energy E_c, where we observe that at least ten partial waves contribute to the observables at the lowest collision energy we consider later in this paper ($E_c = 100 \, \text{K}$). As a
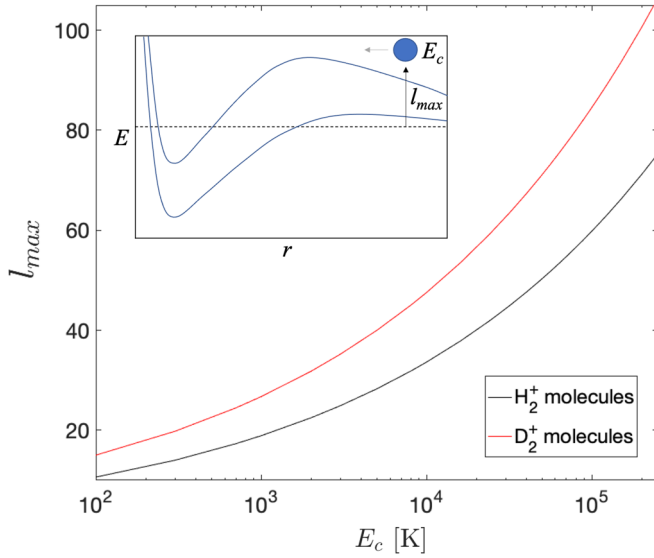
FIG. 2. Maximum number of partial waves (l_{max}) versus collision energy (E_c) as calculated for a Langevin impact parameter. The concept figure in the inset is illustrative of the maximum contributing partial wave to an ion-atom collision.

result, quantum mechanical effects are potentially washed out for the range of collision energies explored in this paper, and a classical approach is adequate.

III. RESULTS AND DISCUSSION

Three-body recombination processes involving hydrogen and deuterium species are considered simultaneously throughout this section.

The pairwise additive approximation is used to describe the overall potential of the three-body systems under study. A similar approach has been proven successful in cold chemistry [11,30,33], ion mobility experiments [29], and van der

Waals molecular formation [19]. Here, atom-atom interactions are modeled by a Lennard-Jones potential: $U(r) = C_{12}/r^{12} - C_6/r^6$, with $C_6 = 6.499$ a.u. [34] and dissociation energy $D_e^{H_2} = 36118.11$ cm^{-1} ($D_e^{D_2} = 36748.38$ cm^{-1} for deuterium) [35] that correlates with the $X\,^1\Sigma_g$ electronic state. Ion-atom interactions are described by the model potential $U(r) = C_8/r^8 - C_4/r^4$ that correlates with the $X\,^2\Sigma_g^+$ electronic state with dissociation energy $D_e^{H_2^+} = 21379.35$ cm^{-1} ($D_e^{D_2^+} = 21711.64$ cm^{-1} for deuterium) [35] and $C_4 = \alpha/2$, where α denotes the static dipole polarizability of hydrogen ($\alpha = 9/2$ a.u. [36]).

The energy-dependent ion-atom-atom three-body recombination rates $k_3(E_c)$ are depicted in Fig. 3, where a factor of $1/4$ has been included to account for the different spin states of the interaction [31]. Notably, $k_3(E_c)$ is almost two orders of magnitude larger for the formation of the molecular ion compared to that of the molecule, which is expected given the stronger nature of interactions for the former. Two power-law behaviors are identified for each species formation, and the change in trend is established around the dissociation energy D_e of the molecule or molecular ion products. The same behavior was noted for the formation of van der Waals molecules X-RG (where RG is a rare gas atom) through three-body recombination [19]. Here, Mirahmadi and Pérez-Ríos showed that the change in trend could be attributed to an interplay between the contributions of the X-RG potential's short- and long-range tails to the molecule formation, depending on the energy of the system. Based on this, we distinguish low-energy and high-energy regimes in Fig. 3, with a steeper trend characterizing the high-energy region. In that respect, the long-range tail of the potential plays an important part in the formation of molecules at low collision energies, and the opposite is true for the short-range tail.

A power law for the molecular ion recombination rate at low energies was inferred from Fig. 3, yielding
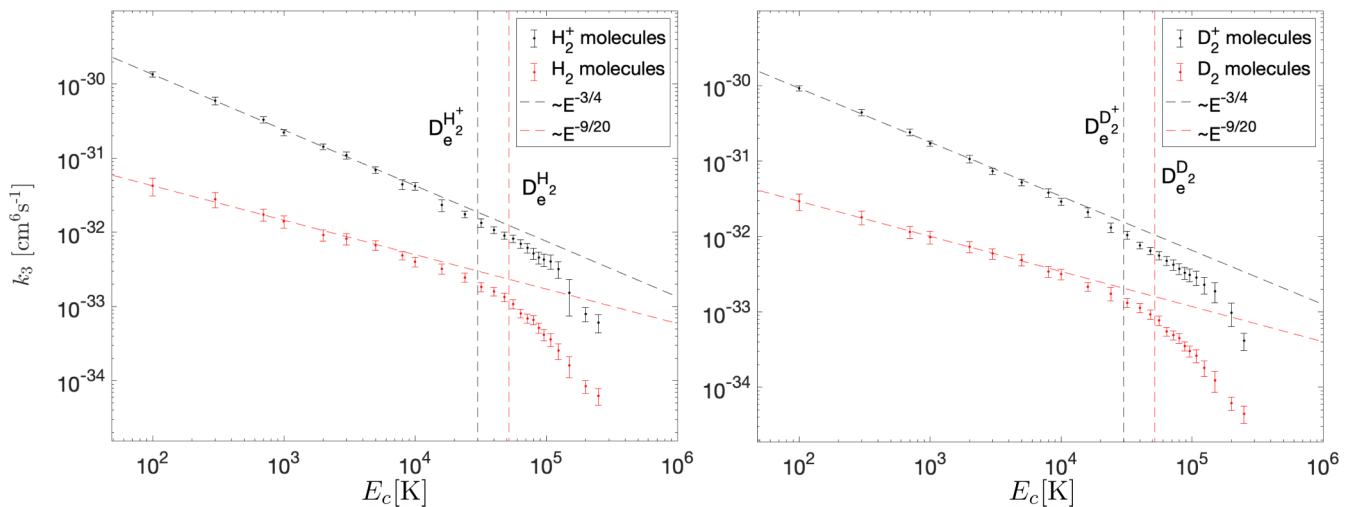
$$k_3 \sim E_c^{-3/4}. \tag{8}$$

FIG. 3. Energy-dependent ion-atom-atom three-body recombination rates for the hydrogen and deuterium plasmas. The black symbols depict the rate of molecular ion formation, whereas the red symbols describe the formation of molecules. The error bars attached to each symbol account for one standard deviation error as customary in Monte Carlo simulations [see Eq. (6)]. The vertical lines in the left panel represent the dissociation energies of H$_2^+$ and H$_2$, whereas, in the right panel, the vertical lines represent the same observable for D$_2^+$ and D$_2$.
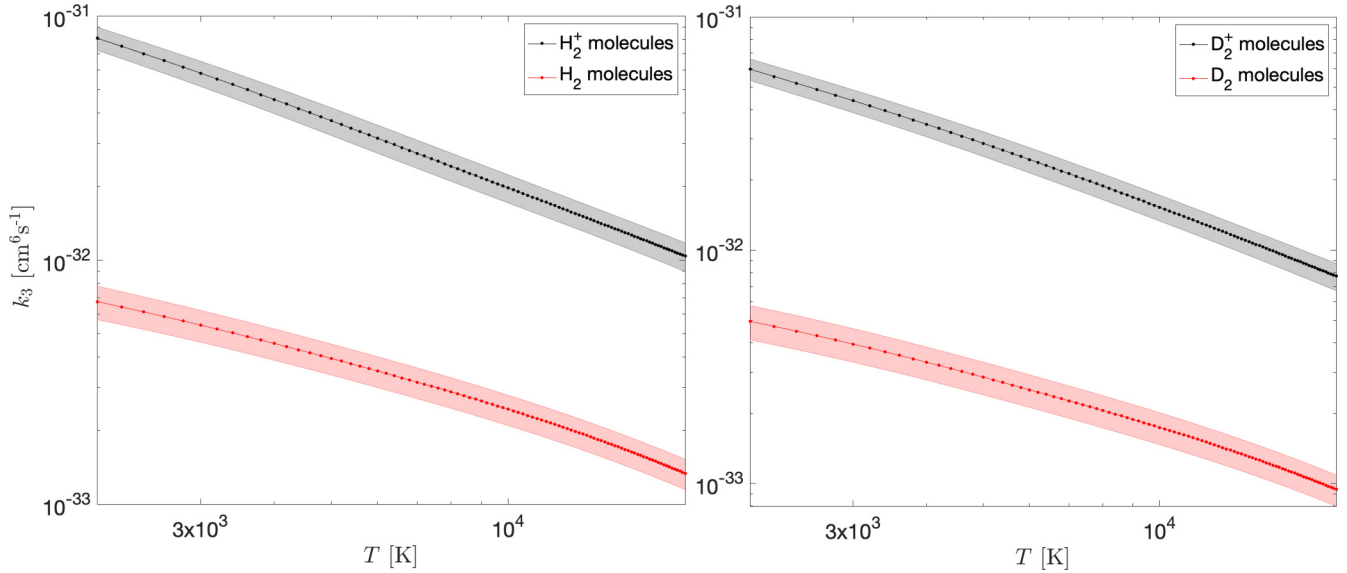
FIG. 4. Thermally averaged ion-atom-atom three-body recombination rates for hydrogen (right panel) and deuterium plasmas (left panel). The black symbols depict the rate of molecular ion formation, whereas the red symbols describe the formation of molecules. The shades account for one standard deviation error as customary in Monte Carlo simulations [see Eq. (6)].

In fact, this low-energy power law behavior for the formation of molecular ions through three-body recombination was devised in multiple other systems [28] and was also derived by Smirnov in 1967, who treated three-body recombination as a two-step chemical process [37].

In a different vein, the rate for molecule formation follows a less steep trend and is defined by the following power law:

$$k_3 \sim E_c^{-9/20}, \tag{9}$$

which is very close to the expected behavior for a three-body recombination process dominated by a potential $\propto r^{-5}$. However, any of the interatomic potentials included in our calculations show this long-range behavior.

Furthermore, it is worth investigating the thermal averaged three-body recombination rate at temperatures $2000\,\mathrm{K} \leqslant T \leqslant 20\,000\,\mathrm{K}$. The thermal average is obtained via integrating the energy-dependent three-body recombination rate in Eq. (5) over the appropriate Maxwell-Boltzmann distribution of collision energies,

$$k_3(T) = \frac{1}{2(k_B T)^3} \int_0^\infty k_3(E_c) E_c^2 e^{-E_c/(k_B T)} dE_c, \tag{10}$$

where k_B is the Boltzmann constant. The changes in the thermal-averaged rates with temperature for the molecule and molecular ion species are presented in Fig. 4. Comparing the data in Fig. 4 to those in Fig. 3, it is first noticeable how the trends follow different power laws. This is expected given the effect of thermal averaging on the contribution of different collision energies at a given temperature T. Hence, the bending at the dissociation energy washes out and becomes recognizable to a smaller degree, while the power laws describing the trends shift to higher exponent values.

The effect of the mass of the participating species on the dynamics of the recombination process is beautifully exposed by the three-body approach we adopt and is majorly defined by Eq. (5). Precisely, Fig. 4 reveals a factor of $\sqrt{2}$ difference

between the magnitudes of the rates for hydrogen and deuterium, which agrees with the prediction of Eq. (5).

In fusion divertor plasmas, in the detachment divertor regime, where $T \sim 1\,\mathrm{eV}$, $k_3(T) \sim 10^{-32}\mathrm{cm}^6/\mathrm{s}$ (see Fig. 4), and assuming a gas density $\rho \sim 10^{15}\,\mathrm{cm}^{-3}$ [38], the collisional rate

$$\Gamma = k_3(T)\rho^2, \tag{11}$$

is $\sim 0.01\,\mathrm{s}^{-1}$. Therefore, ion-atom-atom three-body recombination may not play a relevant role in volumentric plasma recombination processes. However, ion-atom-atom three-body recombination has a smoother temperature dependence than the most prominent three-body recombination process in volumetric recombination: $e + e + \mathrm{H}^+ \rightarrow \mathrm{H} + e$ or $e + e + \mathrm{D}^+ \rightarrow \mathrm{D} + e$, which goes like $T^{-9/2}$ [39]. Therefore, at higher plasma temperatures, ion-atom-atom three-body recombination may start to play a relevant role in the plasma dynamics.

IV. SUMMARY AND CONCLUSIONS

This paper presents a first-principles calculation of the ion-atom-atom three-body recombination rate in deuterium and hydrogen plasmas. Our approach is based on a classical trajectory calculation in hyperspherical coordinates, supported by the large number of partial waves contributing to the atom-ion scattering. The main result is the formation of molecular ions, i.e., H_2^+ and D_2^+ in cold hydrogen and deuterium plasmas, respectively, to the detriment of neutral species. Furthermore, we find a specific change of trend in the three-body recombination rate as a function of collision energy around the dissociation energy of the molecular ion, which correlates with the role of short-range physics in the reaction dynamics.

The collisional rate associated with three-body recombination is $\sim 0.01\,\mathrm{s}^{-1}$ in typical fusion divertor plasmas conditions, which is a relatively slow process compared with other volumetric recombination mechanisms. However, the

situation may change at higher temperatures since ion-atom-atom three-body recombination shows a weaker temperature dependence than other three-body volumetric recombination processes. Finally, it is worth mentioning that the current approach could be extended to treat more involved three-body processes like $H_2^+ + H + H \rightarrow H_3^+ + H$, which may play a significant role in plasma physics.

[1] B. D. Esry, C. H. Greene, and J. P. Burke, Phys. Rev. Lett. **83**, 1751 (1999).

[2] J. Weiner, V. S. Bagnato, S. Zilio, and P. S. Julienne, Rev. Mod. Phys. **71**, 1 (1999).

[3] P. F. Bedaque, E. Braaten, and H.-W. Hammer, Phys. Rev. Lett. **85**, 908 (2000).

[4] H. Suno, B. D. Esry, and C. H. Greene, New J. Phys. **5**, 53 (2003).

[5] T. Weber, J. Herbig, M. Mark, H.-C. Nägerl, and R. Grimm, Phys. Rev. Lett. **91**, 123201 (2003).

[6] M. Schmidt, H.-W. Hammer, and L. Platter, Phys. Rev. A **101**, 062702 (2020).

[7] C. H. Greene, P. Giannakeas, and J. Pérez-Ríos, Rev. Mod. Phys. **89**, 035006 (2017).

[8] J. Pérez-Ríos, Mol. Phys. **119**, e1881637 (2021).

[9] H. Hirzler, E. Trimby, R. S. Lous, G. C. Groenenboom, R. Gerritsma, and J. Pérez-Ríos, Phys. Rev. Research **2**, 033232 (2020).

[10] J. Pérez-Ríos and C. H. Greene, J. Chem. Phys. **143**, 041105 (2015).

[11] A. Krükow, A. Mohammadi, A. Härter, J. H. Denschlag, J. Pérez-Ríos, and C. H. Greene, Phys. Rev. Lett. **116**, 193201 (2016).

[12] N. Brahms, B. Newman, C. Johnson, T. Greytak, D. Kleppner, and J. Doyle, Phys. Rev. Lett. **101**, 103002 (2008).

[13] H. Suno and B. D. Esry, Phys. Rev. A **80**, 062702 (2009).

[14] N. Brahms, T. V. Tscherbul, P. Zhang, J. Kłos, H. R. Sadeghpour, A. Dalgarno, J. M. Doyle, and T. G. Walker, Phys. Rev. Lett. **105**, 033001 (2010).

[15] N. Brahms, T. V. Tscherbul, P. Zhang, J. Kłos, R. C. Forrey, Y. S. Au, H. R. Sadeghpour, A. Dalgarno, J. M. Doyle, and T. G. Walker, Phys. Chem. Chem. Phys. **13**, 19125 (2011).

[16] Y. Wang, J. P. D'Incao, and B. D. Esry, Phys. Rev. A **83**, 032703 (2011).

[17] N. Tariq, N. A. Taisan, V. Singh, and J. D. Weinstein, Phys. Rev. Lett. **110**, 153201 (2013).

[18] N. Quiros, N. Tariq, T. V. Tscherbul, J. Kłos, and J. D. Weinstein, Phys. Rev. Lett. **118**, 213401 (2017).

[19] M. Mirahmadi and J. Pérez-Ríos, J. Chem. Phys. **154**, 034305 (2021).

[20] M. Mirahmadi and J. Pérez-Ríos, J. Chem. Phys. **155**, 094306 (2021).

[21] D. R. Flower and G. J. Harris, Mon. Not. R. Astron. Soc. **377**, 705 (2007).

[22] R. C. Forrey, Astrophys. J. Lett. **773**, L25 (2013).

[23] S. I. Krasheninnikov, A. Y. Pigarov, D. A. Knoll, B. LaBombard, B. Lipschultz, D. J. Sigmar, T. K. Soboleva, J. L. Terry, and F. Wising, Phys. Plasmas **4**, 1638 (1997).

[24] S. I. Krasheninnikov and A. S. Kukushkin, J. Plasma Phys. **83**, 155830501 (2017).

[25] A. Kukushkin, S. Krasheninnikov, A. Pshenov, and D. Reiter, Nucl. Mater. Energy **12**, 984 (2017), Proceedings of the 22nd International Conference on Plasma Surface Interactions 2016, 22nd PSI.

[26] Please note that in general, ion-atom-atom three-body recombination is given by $B + B + A^+$.

[27] J. Pérez-Ríos, S. Ragole, J. Wang, and C. H. Greene, J. Chem. Phys. **140**, 044307 (2014).

[28] J. Pérez-Ríos, *An Introduction to Cold and Ultracold Chemistry* (Springer International Publishing, Cham, 2020).

[29] J. Pérez-Ríos and C. H. Greene, Phys. Rev. A **98**, 062707 (2018).

[30] A. Mohammadi, A. Krükow, A. Mahdian, M. Deiß, J. Pérez-Ríos, H. da Silva, M. Raoult, O. Dulieu, and J. H. Denschlag, Phys. Rev. Research **3**, 013196 (2021).

[31] P. S. Krstić, R. K. Janev, and D. R. Schultz, J. Phys. B: At., Mol. Opt. Phys. **36**, L249 (2003).

[32] F. T. Smith, Discuss. Faraday Soc. **33**, 183 (1962).

[33] H. Hirzler, R. S. Lous, E. Trimby, J. Pérez-Ríos, A. Safavi-Naini, and R. Gerritsma, Phys. Rev. Lett. **128**, 103401 (2022).

[34] Z.-C. Yan, J. F. Babb, A. Dalgarno, and G. W. F. Drake, Phys. Rev. A **54**, 2824 (1996).

[35] J. Liu, E. J. Salumbides, U. Hollenstein, J. C. J. Koelemeij, K. S. E. Eikema, W. Ubachs, and F. Merkt, J. Chem. Phys. **130**, 174306 (2009).

[36] P. Schwerdtfeger and J. K. Nagle, Mol. Phys. **117**, 1200 (2019).

[37] B. M. Smirnov, JETP **24**, 1180 (1967).

[38] I. H. Hutchinson, R. Boivin, F. Bombarda, P. Bonoli, S. Fairfax, C. Fiore, J. Goetz, S. Golovato, R. Granetz, M. Greenwald, S. Horne, A. Hubbard, J. Irby, B. LaBombard, B. Lipschultz, E. Marmar, G. McCracken, M. Porkolab, J. Rice, J. Snipes *et al.*, Phys. Plasmas **1**, 1511 (1994).

[39] Y. Sayasov, Bull. Soc. Frib. Sci. Nat. **65**, 76 (1976).